LIQUID CRYSTAL SURFACES

P. Pershan

COLLOQUE DE PHYSIQUE
Colloque C7, supplément au n°10, Tome 50, octobre 1989

LIQUID CRYSTAL SURFACES

P.S. PERSHAN

Physics Department and Division of Applied Sciences, Harvard University, U.S.A.

Abstract

The use of specular reflection of X-rays to study the structure of the liquid-vapor and liquid crystal-vapor interfaces along the direction normal to the surface is described. If $R_F(\theta)$ is the theoretical Fresnel reflection law for x-rays incident on an ideal flat surface at an angle θ and $R(\theta)$ is the measured reflectivity from the true surface, the ratio $R(\theta)/R_F(\theta)$ is a measure of the electron density along the surface normal: i.e.

$$\frac{R(\theta)}{R_F(\theta)} \approx \left| \frac{1}{\rho_\infty} \int \frac{\partial \langle \rho(z) \rangle}{\partial z} e^{iQ_z z} dz \right|^2$$

where ρ_∞ is the electron density far from the surface, $\partial\langle\rho(z)\rangle/\partial z$ is the gradient of the x-y average of the electron density along the surface normal and $Q_z=(4\pi/\lambda)\sin(\theta)$. For the surface of simple liquids like H_2O, the principal observation is that the electron density profile from the bulk to the vapor is dominated by thermally excited capillary waves. For both the isotropic phase and the nematic liquid crystal phase, structure is observed in $R(\theta)$ due to surface induced local smectic order. Depending on the material, layering transitions at the surface of isotropic phases are observed to be either sharp or gradual functions of temperature. The possible interpretation of this in terms of wetting and roughening effects will be discussed. On approaching a 2nd order nematic to smectic A transition, the number of layers diverge in a manner that can be described as critical absorption. Other examples to be discussed include the surface structure of a lytropic liquid crystal and the appearance of surface layers of the tilted hexatic smectic I phase on freely suspended films of a smectic C phase.

Introduction:

The unique character of liquid crystalline phases has facilitated a large number of theoretical and experimental studies on the statistical physics of condensed matter.[1,2] One of the earliest observations from this effort was that the molecular order near surfaces can often be strikingly different from the order in the bulk far from the surfaces.[3-6] The purpose of this paper is to review those surface effects that have been studied by x-ray scattering

techniques. As is the case with all other systems, there are two main classes of surface phenomena. The first, and in many ways the simplest to visualize, is where the surface induces molecular layering that decays with distance from the surface.[7-10] The major part of this review will describe how the angular dependence of x-ray specular reflectivity can be used to study this type of liquid cystalline surface phenomena.[11-18]

A second type of effect, such as surface melting, is observed when the presence of the surface changes the statistical physics such that the molecular order along directions parallel to the surface is measurably different near to the surface than it is in the bulk.[19-23] Much of the interest in this type of phenomena can by attributed to the general effects of dimensionality on statistical physics: e.g. the surface being a two dimensional structure in a three dimensional world. A large fraction of the surface phenomena studied by grazing incidence x-ray, or neutron scattering, on systems other than liquid crystals falls into this category. There have been a number of very interesting liquid crystalline examples of this second type of surface phenomena[24-27] and although we do not have the space to describe them fully in this review we will give one example from our own work. One of the principal differences between liquid crystals and most other systems is that for liquid crystals the necessary surface specificity of x-ray studies can be achieved in transmission on thin free standing liquid crystalline films with large surface to volume ratios, rather than in a grazing incidence geometry on bulk samples. Films as thin as two molecular layers are quite stable and experiments have been done to study structural phase changes as a function of both temperature and film thickness.[28-30]

Specular Reflectivity

Experimental:

Various experimental geometries for the study of specular reflectivity from liquid, or liquid crystalline, systems have been previously reported.[31-34] The basic kinematics of specular reflection are illustrated in Figs. 1 and 2.

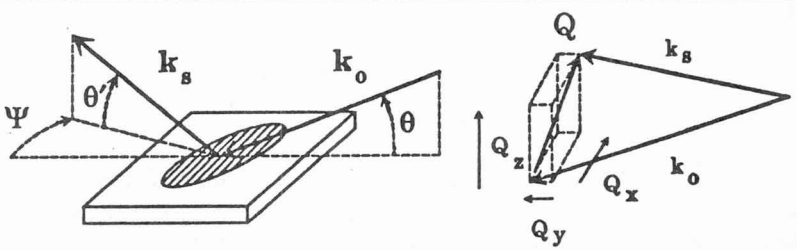

Fig. 1: Kinematics of specular reflection. The Liquid crystal surface is maintained horizontal and the incident wavevector k_0 makes an angle θ to the liquid surface. The detector can be located at angles θ' to the horizontal and Ψ to the plane of incidence. Specular reflection is restricted to the condition θ=θ' and Ψ=0. As implied in the drawing to the right, the specular reflection condition corresponds to the components $Q_X = k_0\cos(\theta')\sin(\Psi)$ and $Q_Y=k_0[\cos(\theta)-\cos(\theta')\cos(\Psi)]$ of the wavevector transfer $\mathbf{Q} = \mathbf{k_S} - \mathbf{k_0}$ being zero.

In view of the fact that the various liquid crystalline phases to be discussed below are relatively fluid, the studies to be described here on the free liquid crystal-vapor interface require that the sample be held horizontal. As such the incident wave vector $\mathbf{k_0}$ is directed downward by an angle θ and the scattered radiation is observed by a detector located such that the wavevector $\mathbf{k_S}$ makes an angle θ' with the horizontal and in a plane that makes an angle ψ with the plane of incidence. The scattering is described by a wavevector transfer $\mathbf{Q} = \mathbf{k_S} - \mathbf{k_0}$ and since the condition for specular reflection requires θ = θ' and ψ = 0 it is only observed when $Q_X = Q_Y = 0$ and $Q_Z \equiv |\mathbf{Q}| = 2k_0\sin(\theta)$. If either θ' or ψ is scanned specular reflection is observed as a sharp peak superposed on a broad background of diffuse scattering.

There are different techniques for achieving this kinematics depending on the nature of the source. In the case of horizontally incident synchrotron radiation, the beam can be bent downward by rotating the reciprocal lattice vector of the monochromator G along a cone such that the component of G parallel to the direct beam from the

synchrotron is held fixed (e.g. $\mathbf{G} \bullet \mathbf{k}_i$ = constant). In this geometry, illustrated in Fig. 2, $2\Theta_0 = \sin^{-1}(\lambda G/4\pi)$ is the Bragg angle of the monochromator for wavelength λ. The component of G perpendicular to the incident Synchrotron beam, $G\cos(\Theta_0)$ *is rotated about the horizontal incident synchrotron beam* by an angle χ such that the Bragg vector G points down from the horizontal by an angle τ: i.e. $\sin(\tau) = \sin(\Theta_0)\sin(\chi)$. Since the wavelength of the reflected radiation λ is fixed the downward angle for $\mathbf{k}_0$ is $\theta = \sin^{-1}[\lambda G\sin(\tau)/2\pi]$. As the monochromator is tilted the loci of the end points of $\mathbf{k}_0$ follow a cone and for a downward angle θ the projection of $\mathbf{k}_0$ on the horizontal (i.e. line B) makes an angle $2\Theta_1 = 2\Theta_0 - \Phi$: i.e. Θ_0 is the direction of the beam $\mathbf{k}_0$ when $\tau=\chi=0$. The angle $\Phi = 2\Theta_0 - 2\Theta_1$ is obtained from conservation of wavevector in the horizontal plane:

$$(G\cos(\tau))^2 = k_0^2 + (k_0\cos(\theta))^2 - 2k_0^2\cos(\theta)\cos(2\Theta_1).$$

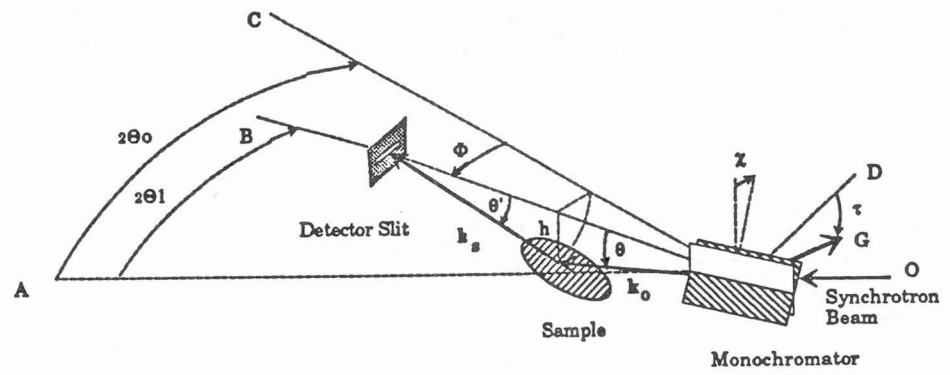

Fig. 2: Schematic illustration of geometry for measurement of specular reflectivity using synchrotron radiation. Details are described in the text.

The sample must be lowered an amount $h = L\tan(\theta)$ where L, not shown, is the distance from the monochromator to the center of the sample. In the experiments to be described below L is typically of the order of 600mm such that an angle $\theta\approx3°$, corresponding to $Q_z\approx0.43\text{Å}^{-1}$ for $\lambda\approx1.54\text{Å}$, requires $h \approx 31$mm. At this angle the plane containing the monochromator, the sample and the detector must be rotated about at vertical axis through the center of the monochromator by $\Phi = 2\Theta_0 - 2\Theta_1$. For a wavelength $\lambda \approx 1.54\text{Å}$ and a Ge(111) crystal monochromator $G\approx1.927\text{Å}^{-1}$, the untilted Bragg angle $\Theta_0 \approx 13.66°$, and the downward angle $\theta \approx 3°$ requires $\tau\approx 6.19°$, $\chi\approx 6.37°$, and $\Phi = 2\Theta_0 - 2\Theta_1 \approx 0.38°$. If the distance between the sample and the detector slit is equal to the distance between the sample and the monochromator, specular reflection is observed without any vertical motion of the detector. In practice the dimensions of detector slit are large enough to intercept the entire direct beam at $\theta = \Phi = 0$ when the sample is removed. For a flat sample a scan of the position of the detector slit, in either the horizontal or vertical directions, obtains a line shape that is the superposition of the line shape observed on scanning the detector through the direct beam on top of a broad background due to diffuse scattering. The sample position and the flatness of the surface can be monitored by scanning the detector position for a series of different sample heights.

Theoretical Background:

The principal theoretical expression relevant to the measurements of specular reflectivity is presented as Eq. 1.[16,18,35-37] If $R(Q_z)$ is the predicted reflectivity for a real surface and $R_F(Q_z)$ is the theoretical reflectivity from an idealized sharp interface, then for incident angles $\theta \geq$ (4 or 5) times the critical angle $\theta_c = \sqrt{\rho_\infty e^2\lambda^2/\pi mc^2}$:

Eq. 1 $$\frac{R(Q_z)}{R_F(Q_z)} = \left| \frac{1}{\rho_\infty} \int dz \frac{\partial\langle\rho\rangle}{\partial z} e^{iQ_z z} \right|^2$$

where $Q_z = (4\pi/\lambda)\sin(\theta)$ is defined in terms of the x-ray wavelength λ, ρ^∞ is the average electron density in the bulk liquid and $\partial\langle\rho\rangle/\partial z$ is the derivative along the normal to the surface of the average electron density. Even though Eq. 1 can not be formally justified, as $\theta \to \theta_c$ there are many surface profiles for which the measured $R(Q_z) \to R_F(Q_z)$ as $Q_z \to 0$. Since according to Eq. 1 $R(Q_z)/R_F(Q_z) \to 1$ as $Q_z \to 0$ the result is often applicable over all angles.

Neglecting absorption effects, which are only important for $\theta \approx \theta_c$, when $\theta >> \theta_c$

Eq. 2 $$R_F(Q_z) = \left| \frac{\theta - \sqrt{\theta^2 - \theta_c^2}}{\theta + \sqrt{\theta^2 - \theta_c^2}} \right|^2 \approx \left| \frac{\theta_c}{\theta + \sqrt{\theta^2 - \theta_c^2}} \right|^4 .$$

Eq. 1 is simply derived in the kinematic approximation by calculating the amplitude of scattered radiation due to the electrons in a thin layer δz at some height z above, or below the average surface. Neglecting polarization effects for convenience, at some large distance $\mathbf{r}$ from the sample, the ratio of the scattered field δE^s from a layer of infinitesimal thickness δz to the incident field E^0 is approximately:

Eq. 3 $$\frac{\delta E^s}{E^0} \approx \frac{e^2}{mc^2} \delta z \left\{ \frac{1}{r} \int dx dy [\rho(x,y,z)] e^{i[\mathbf{k}^s - \mathbf{k}^0] \cdot \mathbf{r}} \right\}$$

where $\mathbf{k}^0$ and $\mathbf{k}^s$ are the incident and scattered wavevectors respectively. Writing $\rho(x,y,z) = \langle\rho(z)\rangle + [\rho(x,y,z) - \langle\rho(z)\rangle]$ the integral of the first term obtains

Eq. 4 $$\left(\frac{\delta E^s}{E^0}\right)^{1st\ term} \approx \frac{e^2}{mc^2} \left\{ \frac{4\pi^2 \delta(k^s_x - k^0_x)\delta(k^s_y - k^0_y)}{r} \right\} (\langle\rho(z)\rangle \delta z) e^{i(k^s_z - k^0_z)z} .$$

The functions $\delta(k^s_y - k^0_y)$ and $\delta(k^s_x - k^0_x)$ correspond respectively to the two conditions for specular reflection: namely that the incident and reflected angles must be equal, and the reflected beam must be in the incident plane. The result displayed in Eq. 1 is obtained by integrating Eq. 4 by parts over z.The second term gives rise to diffuse scattering effects that we do not discuss in this paper.[36-41]

The physical significance of Eq. 1 is illustrated by two examples. The dashed line in Fig 3a illustrates an electron density profile $\langle\rho(z)\rangle$ that has been found for simple liquids such as H_2O, CH_3OH, CCl_4 and the isotropic phase of liquid crystals at temperatures sufficiently high.[36,37] If the derivative is approximated as

Eq. 5 $$\frac{1}{\rho^\infty} \frac{\partial\langle\rho\rangle}{\partial z} \approx \frac{1}{\sqrt{2\pi\sigma^2}} e^{-z^2/2\sigma^2} ,$$

where σ is a parameterization of the root mean square width of the surface profile, the predicted reflectivity is $R(Q_z)/R_F(Q_z) \approx \exp(-Q_z^2\sigma^2)$. Agreement with this model is illustrated in Fig. 3c. The open squares are the calculated ratio between the measured $R(Q_z)$ and the Fresnel form $R_F(Q_z)$ shown in Fig. 3b. The solid line through the data in Fig. 3c is the Gaussian form (Eq. 5) with a value of $\sigma \approx 2.7$Å that is in very good agreement with the predictions of thermally excited capillary waves.[42-44] The reflectivity data for water shown in Fig. 3b extended over more than eight orders of magnitude. In this particular case the precision with which the data can be said to agree with Eq. 5, as well as the precision with which σ is determined, are both related to the maximum value of Q_z that can be reached. Since the reflectivity falls rapidly with increasing Q_z the high brilliance of synchrotron radiation sources is essential for reaching the largest Q_z, and thus attaining the highest spatial resolution.

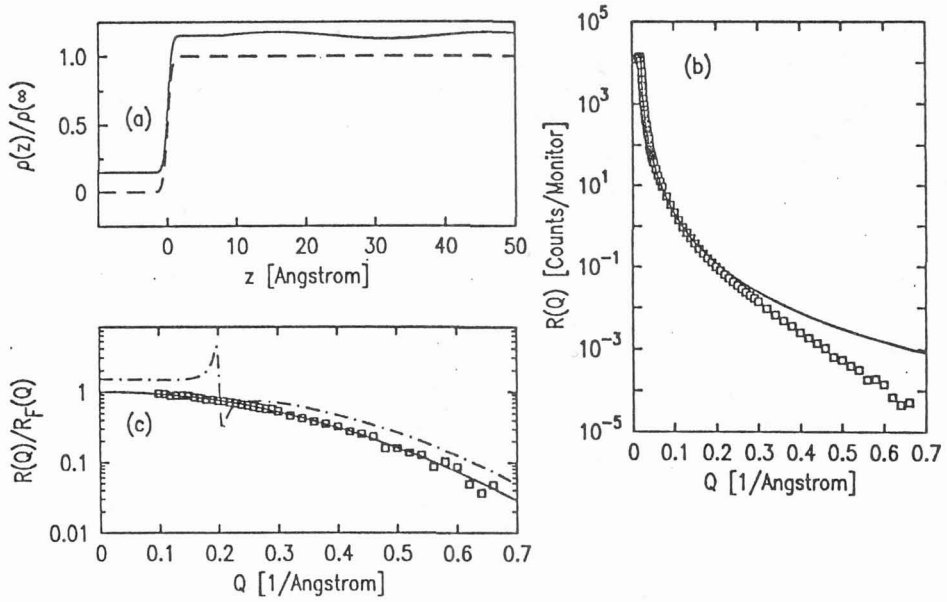

Fig. 3 (a)The broken line illustrates a profile that might be typical of those found for simple liquids like H_2O, CH_3OH, CCl_4 and the isotropic phase of liquid crystals at temperatures sufficiently high. The solid line (displaced for clarity) illustrates a possible profile in which the surface has induced some layering in the electron density. (b) $R(Q_z)$ from a surface of clean H_2O in which the surface tension is measured to be 72.3 dynes/cm: open circles are the data and the solid line is the theoretical $R_F(Q_z)$ given by Eq. 2 and discussed in the text.[42,43] (c) The symbol (□) is ratio $R(Q_z)/R_F(Q_z)$ for the H_2O data in (b). The solid line through the data is the Gaussian (Eq. 5) that best fits the data. The broken line, displaced for visibility, indicates the $R(Q_z)/R_F(Q_z)$ predicted for a layered surface like that shown by the solid line in(a).

The solid line in Fig. 3a illustrates the electron density profile that could possibly describe a surface in which surface induced layering with period L≈30Å that decays exponentially with distance from the surface. A simple guess for the form of this profile is:

Eq. 6
$$\frac{1}{\rho^{\infty}}\frac{\partial\langle\rho\rangle}{\partial z} \approx \frac{1}{\sqrt{2\pi\sigma^2}} e^{-z^2/2\sigma^2} + \left\{\frac{\partial\theta(z-z_0)}{\partial z} B_s e^{[-(z-z_0)/\xi]} \sin[2\pi(z-z_0)/L]\right\}$$

where

$$\theta(z-z_0) \equiv \begin{cases} 0 \text{ if } z < z_0 \\ 1 \text{ if } z \geq z_0 \end{cases}$$

and z_0 specifies the phase of the layers relative to the surface. The Fourier transform of Eq. 6

Eq. 7
$$\Phi(Q_z) \equiv \int dz \frac{1}{\rho^{\infty}}\frac{\partial\langle\rho\rangle}{\partial z} e^{(iQ_z z)} = \Phi_0 + \Phi_1$$

where

$$\Phi_0 \equiv e^{-Q_z^2\sigma^2/2}$$

$$\Phi_1 \equiv i\left(\frac{B_s}{2}\right) e^{-iQ_z z_0}\left\{\frac{\xi Q_0 - 1}{(Q_z - Q_0)\xi - i} - \frac{\xi Q_0 + 1}{(Q_z + Q_0)\xi + i}\right\}.$$

The predicted ratio

Eq. 8 $$\frac{R(Q_z)}{R_F(Q_z)} = |\Phi_0 + \Phi_1|^2$$

contains a Lorentzian like peak due to the Φ_1 term when $Q_z \approx Q_0 = 2\pi/L$ with a width $\Delta Q_z \approx 2/\xi$ (i.e. full width at half maximum). The broken line in Fig. 3c indicates the ratio $R(Q_z)/R_F(Q_z)$ predicted by Eq. 8 in the case that the density oscillations are described by Eq. 6. The detailed shape of the peak at $Q_z = Q_0$ resulting from interference between Φ_0 and Φ_1, depends on the phase z_0 and the amplitude of B_s. The reflectivity observed from the free surfaces of liquid crystals displays these features although, as will be shown below, there are differences between this form and the observations that imply that the region near the surface is different from the details of this simple model.[16,18]

Liquid Crystals

Thermotropic Liquid Crystalline Phases:

The most common type liquid crystalline materials, like those found in various display devices, are organic molecules consisting of a rigid central core with relatively flexible alkane chains at one, or both ends.[45,46] A typical example from the isomorphic series designated as nO.m is illustrated in Fig. 4a for n=4 and m=8. Fig. 4b illustrates the chemical structure for a 4-cyano-4'-nonylbiphenyl (9CB) from the isomorphic series nCB. A similar series with the alkyl chain replaced by an alkoxy chain is referred to as nOCB.

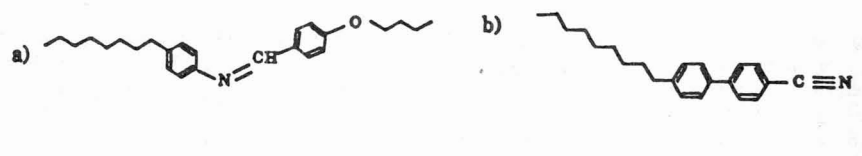

Fig. 4 (a)Chemical structure for the liquid crystalline forming molecules n-(4-butyl)oxybenzylidene)-4'-(n-octyl)aniline (4O.8)[47] and (b) for 4-cyano-4'-nonylbiphenyl (9CB).[48]

Although the flexibility of the alkane chains certainly plays an important role in stabilizing the various liquid crystalline phases their structure can be understood by imagining the molecules to be rigid rods, of the order of 30Å long and 4Å to 5Å in diameter.[49-51] Above ~ 79°C, in bulk samples of 4O.8, the molecules are randomly oriented and the sample is an isotropic liquid. On cooling below ~ 79°C the system undergoes a first order transition to an optically birefringent phase in which the molecules are parallel to one another. In this nematic phase, although there is long range order in the molecular orientation, there is not any long range order in the molecular positions and the nematic is an anisotropic fluid phase.[1] The nematic order parameter is usually defined as $S = \langle 3\cos^2(\phi) - 1\rangle/2$ where ϕ is the angle between the long axis of the molecular rod and macroscopic symmetry axis.

On cooling further 4O.8 undergoes a second order transition at ~ 64°C to a smectic A phase in which the molecules are organized in layers. The simplest manifestation of the layering is the observation of sharp "Bragg like" peaks in the x-ray scattering cross section at scattering vectors $Q = 2\pi/L$ where, for the 4O.8 molecule, L is approximately equal to the length of the molecule.[52-54] Molecules from the nCB series form layers in which molecules partially overlap each other and L≈1.6 times the molecular length.[55,56]

DeGennes developed a Landau type mean field theory to describe the nematic and smectic A phase transitions in which the smectic order parameter Ψ is related to the density $\rho(r)$ by:

Eq. 9 $$\rho(r) = \langle\rho\rangle + \mathrm{Re}\left\{\Psi e^{iQ_0 \cdot r}\right\}$$

where Ψ is the smectic order parameter and $Q_o = (2\pi/L)\hat{z}$.[57,58] Fluctuations in the phase of the complex order parameter Ψ correspond to fluctuations in the position of the smectic layers. The leading terms in the expansion of free energy density in powers of Ψ and S have the form:

Eq. 10
$$F = \frac{1}{2}a(T-T_{NA})|\Psi^2| + \frac{1}{4}b|\Psi^4| + \frac{1}{2}\left|\frac{\partial\Psi}{\partial z}\right|^2 + \frac{\eta}{2}\left\{\left|\frac{\partial\Psi}{\partial x}\right|^2 + \left|\frac{\partial\Psi}{\partial y}\right|^2\right\}\ldots$$
$$\frac{1}{2}A(T-T^*)S^2 - \frac{1}{3}BS^3 + \frac{1}{4}C\,S^4 - \kappa S|\Psi^2|\ldots$$

If κ were zero smectic order would appear via a second order transition at $T=T_{NA}$ with $|\Psi| = \sqrt{a(T_{NA}-T)/b}$. Nematic order appears via a first order transition at $T_{IN} = T^* + 2B/9CA$ with $S^o = 2B/3C + \sqrt{2A(T_{IN}-T)}$. Although T_{IN} is usually greater than T_{NA} there are systems in which the transition from the isotropic to smectic A phase is direct, without any nematic phase. The first order isotropic to nematic transition arises since the 4th order polynomial in S has local minima at both S=0 and at S^o and for $T<T_{IN}$ the minima at $S^o \neq 0$ corresponds to the lower energy density. The finite value of κ induces coupling between $|\Psi|$ and S that changes the value of S at the second local minimum by an amount $\delta S^o \propto \frac{1}{2}\chi\kappa|\Psi|^2$ where χ is the nematic response function. When F is evaluated at $S=S^o+\delta S^o$ there can be negative terms proportional to $|\Psi|^4$ and if χ is large enough these terms can be larger than the positive $b|\Psi|^4/4$ term. In this case the net sign of the $|\Psi|^4$ term is negative and the smectic A phase transition is first order.

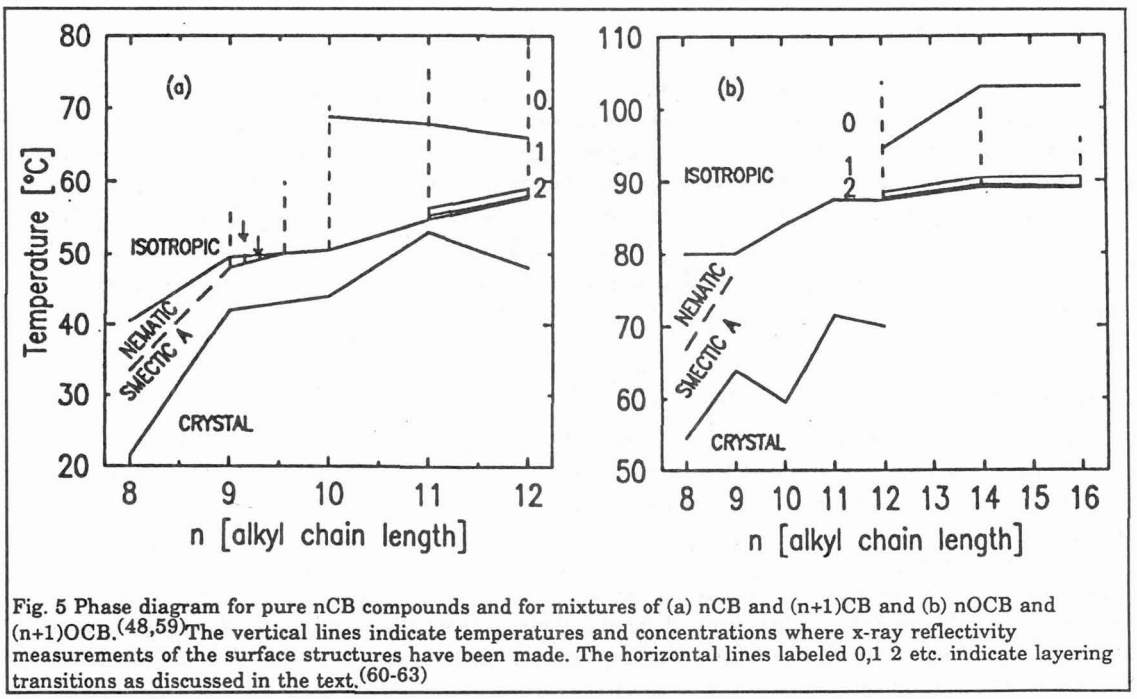

Fig. 5 Phase diagram for pure nCB compounds and for mixtures of (a) nCB and (n+1)CB and (b) nOCB and (n+1)OCB.[48,59] The vertical lines indicate temperatures and concentrations where x-ray reflectivity measurements of the surface structures have been made. The horizontal lines labeled 0,1 2 etc. indicate layering transitions as discussed in the text.[60-63]

Even after renormalization effects are taken into account there remain some serious discrepancies between experiments and the predictions of this theory. Nevertheless, the mean field theory does provide a qualitative description of most of the phenomenology of the isotropic/nematic/smectic A phase sequence. For example, when $T_{IN} - T_{NA}$ is large, $S^o(T)$ is partially saturated in the vicinity of T_{NA}, the response function $\chi(T_{NA})$ is small and the nematic to smectic A transition is usually 2nd order. This is the case for the 4O.8 molecule illustrated in Fig. 4a and for molecules from the nCB series for $n \leq 9$. For mixtures of 4-cyano-4'-nonylbiphenyl (9CB) and 4-cyano-4'-decylbiphenyl (10CB), corresponding to a mean alkane length <n> of between 9 and 9.55, $(T_{IN} - T_{NA})$ is smaller, approaching zero at n≈9.55, the response function χ is larger, and the nematic to smectic A transition is first order. Fig. 5 illustrates the phase diagram for both pure nCB compounds and for mixtures of nCB and

(n+1)CB. For n ≥9.55 the nematic phase is not observed and the phase transition from the isotropic to smectic A phase is 1st order.

A prediction of the mean field theory that is not accurate concerns the correlation lengths $\xi_{//} = \sqrt{a(T-T_{NA})}$ and $\xi_{\perp} = \sqrt{a(T-T_{NA})/\eta}$. The differential x-ray scattering cross section in the nematic phase predicted by the mean field theory does have the form

Eq. 11 $$\frac{d\sigma}{d\Omega} \simeq \frac{\sigma_0}{1 + \xi_{//}^2(Q_z - Q_0)^2 + \xi_{\perp}^2(Q_x^2+Q_y^2)}$$

that is observed experimentally but, when the nematic to smectic A transition is 2nd order, $\xi_{//} \propto t^{-\nu_{//}}$ and $\xi_{\perp} \propto t^{-\nu_{\perp}}$ are observed to diverge with different powers of reduced temperature $t \equiv (1-T_{NA}/T)$.(54) The values of $\nu_{//}$ and $\nu_{\perp}$ are not simply related to each other nor do they have universal values for different materials. The discrepancy has not been resolved by renormalization.

In view of the existing difficulties in obtaining a quantitatively satisfactory theory for the bulk properties of liquid crystals it is premature to expect a more complete understanding of the surface phenomena. Nevertheless it is pedagogically useful to construct a simple mean field theory of surface induced smectic order. Neglecting coupling between S and Ψ, one approach might be to add a surface term to the energy density F (i.e.Eq. 10) of the form

Eq. 12 $F^S = H\delta(z)(\Psi+\Psi^*)$.

Mean field theories of this type have been worked out for a variety of problems and they always predict that far from the surface the order parameter decays with the bulk correlation length, which for the energy density given by Eq. 10 is just $\xi_{//} = \sqrt{a(T-T_{NA})}$. (10,63) In this approximation, since the surface field is localized to the surface region the thickness of the region of smectic order can only grow in some direct relation to the $\xi_{//}$. If the transition from the nematic to the smectic A, or from the isotropic to smectic A is first order, such that $\xi_{//}$ does not diverge as the transition is approached, the thickness of the smectic region remains finite and there can only be partial, or incomplete wetting. If, however, the surface field is not local, for example if instead of $H\delta(z)(\Psi+\Psi^*)$ there is a surface term

Eq. 13 $$F^S \sim -\frac{H}{z^{\gamma}}|\Psi(z)|^2.$$

The combination of the first term in Eq. 10 and the non-local surface field gives rise to a position dependent transition temperature $T_{NA}(z)$ and the thickness the smectic region will grow as $1/(T-T_{NA})^{1/\gamma}$. In fact coupling between the smectic order parameter Ψ and nematic order parameter S must certainly be taken into account.(64-67)

The microscopic origin of nematic order is generally ascribed to the fact that a larger number of rigid rods can be packed into a fixed volume if the rods are oriented parallel to one another. This is clearly one of the major effects. However, the role of attractive Van der Waals forces and dynamic effects associated with interactions between alkane chains on different molecules is not well understood. We suspect that this might be the dominant effect in the formation of smectic A order.(68) In any event, one thing that is clear is that for temperatures corresponding to the nematic temperature range, molecules like those illustrated in Fig. 4 prefer to be oriented parallel to one another (e.g. S≠0). Optical experiments show that at higher temperatures, corresponding to the isotropic phase, the free liquid-vapor surface enhances this tendency and nematic order can be observed at the liquid-vapor interface.(3,4,69,70) Since nematic order is orientational, rather than positional order, neither x-ray nor neutron scattering are particularly useful techniques for studying this effect.

On the other hand, the average surface defines a reference plane that enhances the tendency, characteristic of the smectic A phase, of molecules near the surface to be next to each other as well as being parallel to each other. We will discuss x-ray experiments on molecules from the nCB series for n ≥ 9.55 demonstrating the temperature

dependent appearance of smectic order at the liquid-vapor interface for temperatures for which the bulk phase is isotropic. The interesting physics to discuss is the manner in which additional layers form with decreasing temperature, the evolution of this behavior with increasing n (e.g. as in nCB) and the maximum number of layers that are observed at the 1st order isotropic to smectic A transition temperature; i.e. is the wetting complete?

We will also describe experiments on the nematic phase in which surface induced smectic A positional order penetrates into the bulk hundreds of layer thicknesses. When the nematic to smectic A transition is 2nd order (i.e. for nCB with n≤9 , 4O.8 and for other molecules) the penetration length is exactly equal to the measured bulk correlation length $\xi_{//}$. Although $\xi_{//}$ diverges as $T \rightarrow T_{NA}$, it does not do it in the manner predicted by the mean field theory.[15,16,18] When the nematic to smectic A transition is 1st order, i.e. for mixtures of (1-x)(9CB) and (x)10CB, with x≤0.5 the penetration length is considerably larger than the bulk correlation length. This suggests that for certain concentrations the smectic A phase may wet the liquid-vapor interface.[60-63]

Lyotropic Liquid Crystalline Phases

The historical difference between thermotropic and lyotropic liquid crystals is that the lyotropic are always mixtures, or solutions, of unlike molecules in which one is a normal liquid that does not form liquid crystal phases in the pure form[71-75] Solutions of soaps and water are prototypical examples and their liquid crystalline phases are often studied at fixed temperature, as a function of relative concentrations of the two species. Fig. 6a displays the chemical structure of the molecule cesium perfluoro-octanoate (CSPFO) that, with water, forms the one lyotropic liquid crystal for which we have done surface studies.[76,77] The fluorocarbon part of the molecule is strongly hydrophobic and in a H_2O solution it aggregates in oblate micelles, like those illustrated in the lower part of Fig. 6b, in which the $-COO^{(-)}Cs^{(+)}$ groups "shield" the flourocarbon parts from the H_2O. For a mixture of approximately equal weights of CsPFO and H_2O there is a sequence of isotropic → nematic → smectic A phase transitions with T_{IN}~50°C and T_{NA}~43°C. The actual transition temperatures decrease by about 10°C for each 10 wt% increase in the water content; however, the difference $T_{IN}-T_{NA}$ ~ 6°C is relatively independent of concentration. One possible model for this phase sequence might be that with decreasing temperature the oblate micelles simply orient to form a lyotropic nematic phase in much the same way that the rigid rods of the

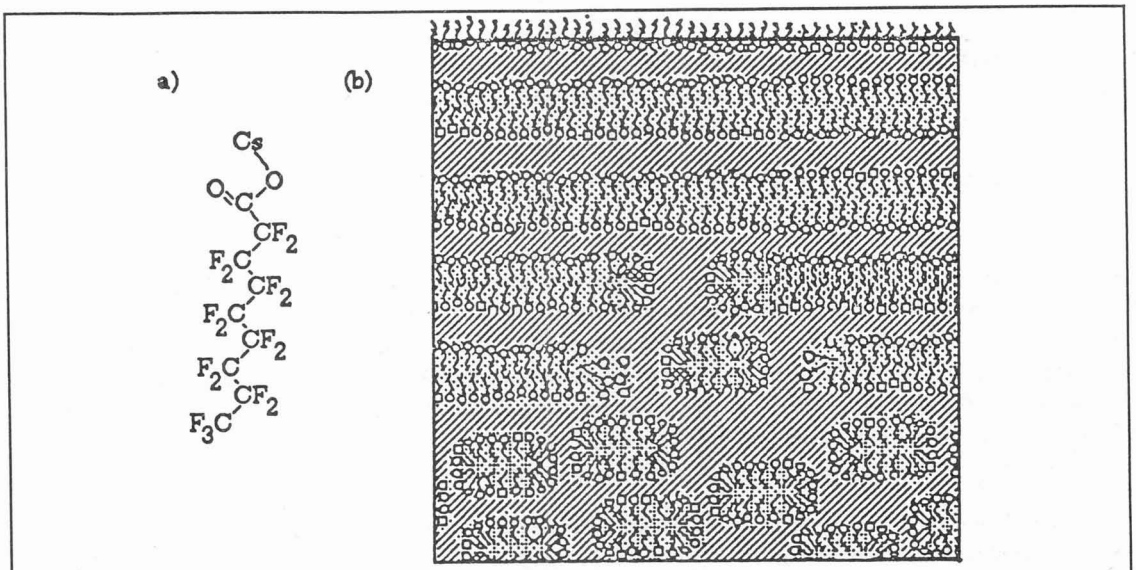

Fig. 6 (a)Chemical structure of the cesium perfluoro-octanoate(CsPFO) molecule. (b) Sketch of one model for the organization of CsPFO molecules in layers near to the surface and in oriented oblate micelles in the bulk, some distance from the surface. The shaded region between the micelles is filled with H_2O.

thermotropic liquid crystals orient to form the thermotropic nematic phase. With decreasing temperature the micelle positions could then align to form the lyotropic smectic A phase. Alternatively, one could also expect that both the size and the shape of the micelles would evolve with temperature and that this might well be what really drives the phase transitions. We will show the results for this system that demonstrate the surface induced smectic order in the nematic phase, near to T_{NA}. One possible model for the surface structure is schematically illustrated in Fig. 6b.

Experimental Results:

Thermotropic Surface Smectic A Order

Fig. 7 displays the ratio of $R(Q_z)/R_F(Q_z)$ for four different liquid crystals as a function of Q_z/Q_o where the smectic layer spacing $L = 2\pi/Q_o$: (a) 8OCB in the nematic phase approximately 0.05°C above a second order nematic to smectic A transition; (b) 9CB in the nematic phase approximately 0.06°C above a tricritical point that separates a region of second order nematic to smectic A transitions from a region of first order transitions; (c) 9.15CB in the nematic phase approximately 0.06°C above a first order nematic to smectic A transition ; and (d) 10CB in the isotropic phase approximately 0.07°C above a first order transition to the smectic A phase. All four cases display structure at $Q_z \approx Q_o$ corresponding to surface induced layering.

For both 8OCB and 9CB the full width at half maximum of the peak is $\Delta Q_z = 2/\xi_{//}(T)$ where $\xi_{//}(T)$ is the critical correlation length of the smectic order parameter as measured separately on bulk samples, or as measured in the reflectivity geometry by scanning the spectrometer (Fig. 2) along Q_z with either Q_x or Q_y tuned slightly off of the specular condition. This is exactly the behavior anticipated in the example illustrated in Fig. 3a,c and described by Eqs. 6, 7 and 8. It is duplicated in all materials for which there is a second order nematic to smectic A transition. It is clear that this is a case of "critical absorption" of the smectic A phase by the free surface. A relatively subtle feature of these data sets that was not anticipated is that the tails of the observed peaks, for Q_z both larger and smaller than Q_o, do not agree with the form of the simple model described by Eq. 6. Close examination of the deviations suggests that the Lorentzian peak appears to be superposed on a "step" such that for $Q_z << Q_o$ the ratio $R(Q_z)/R_F(Q_z)$ is roughly constant and an order of magnitude larger than for $Q_z >> Q_o$.

This feature is due to the fact that the model described by Eq. 6 does not correctly represent the amplitude and phase of the surface induced layering near to the surface. In the absence of theoretical guidance an ad hoc model that can describe the step is obtained by replacing the Gaussian first term in Eq. 6 by

Eq. 14 $$\frac{1}{\rho^{\infty}}\frac{\partial\langle\delta\rho\rangle}{\partial z} \equiv \left\{ \frac{A}{\sqrt{2\pi\sigma_o^2}} e^{-z^2/2\sigma_o^2} + \frac{B}{\pi z} e^{-z^2/2\sigma_1^2} \sin(Q_1 z) \right\}$$

where A and B are defined to ensure that $(\rho^{\infty})^{-1}\int dz(\partial\langle\delta\rho\rangle/\partial z)$ is properly normalized and $Q_1 \approx Q_o$.[16,18] The principal motivation for this form derives from the observation that if $\sigma_1 \to 0$ the Fourier transform of the second term is equal to B for $|Q_z| \leq Q_1$ and zero otherwise. Its main physical content is to emphasize the mathematical observation that by only a slight variation in the layer structure nearest to the surface it is possible to generate the observed step in $R(Q_z)/R_F(Q_z)$ near $Q_z \approx Q_o$. Non-linear least square fits of the data to $R(Q_z)/R_F(Q_z)$ calculated from this model can be used to obtain "best fit" values of $\xi(T)$ and these agree perfectly with values for $\xi_{//}(T)$. Best fit values for other parameters are not necessarily physically significant.

Mixtures of 9CB and 10CB with average alkane lengths between 9 and ~9.55 exhibit first order nematic to smectic transitions. As a function of decreasing temperature, on approaching the transition to the smectic A phase both x-ray scattering and heat capacity studies on bulk samples indicate pretransition growth of the smectic correlations, similar to those found for second order transitions. The growth is cut off at a finite value $\xi_{//}(T_{NA})$ by the first order transition.[48,54] Fig. 8 displays values for $\xi(T)$, obtained from the surface peak measured in specular refection, for both 9.15CB and 9.30CB and $\xi_{//}(T)$, obtained from line shape of critical diffuse scattering

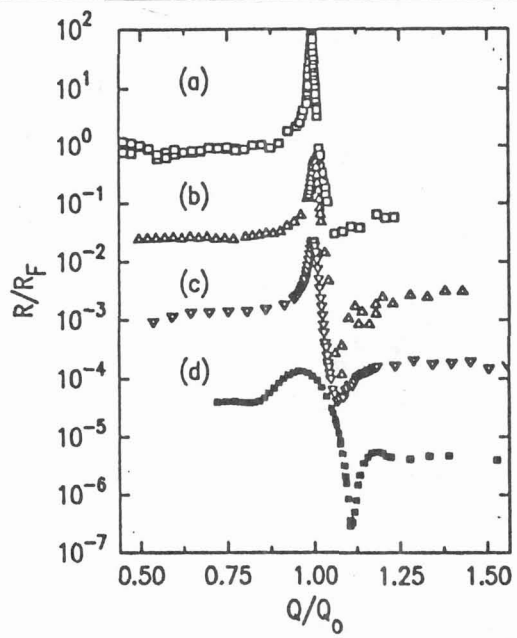

Fig. 7: The ratio of $R(Q_z)/R_F(Q_z)$ for (a)8OCB, (b) 9CB, (c) 9.15CB and (d) 10CB as a function of Q_z/Q_0 at temperatures approximately 0.05°C to 0.06°C above the smectic A transition temperature. The values of Q_0 are respectively (a) 0.0218Å^{-1}, (b) 0.0212Å^{-1}, (c) 0.0206Å^{-1}, and (d) 0.0213Å^{-1} .

from the bulk, measured by tuning the spectrometer off of the specular condition. The values for $\xi_{//}(T)$ agree with independent measurements on bulk samples. In both cases the surface penetration length $\xi(T)$ is longer than the bulk correlation length $\xi_{//}(T)$ and the ratio increases as $T \rightarrow T_{IA}$. Neither of these data sets appear to be examples of a true wetting transition that would be characterized by a divergence in $\xi(T)$ for a finite $\xi_{//}(T)$, and although true wetting should be observed on approaching the tricritical point along the 1st order nematic to smectic A transition line the data suggest that for the nCB series it might be difficult to achieve the necessary temperature and angular resolution to demonstrate the phenomenon. Other materials might be better candidates.

The angular dependence of the specular reflectivity data for 10CB is qualitatively different from the others shown in Fig. 7 in that the peak is broader, not as intense, and most importantly there are subsidiary maxima at Q_z larger and smaller than Q_0. This is shown more clearly in Fig. 9 where we display $R(Q_z)/R_F(Q_z)$ for 10CB, 11CB and 12CB at $T\text{-}T_{IA} \sim 0.01$°C and for 1.0°C.
Since the isotropic to smectic A transition is 1st order, and since the bulk susceptibility for smectic order in the isotropic phase is small, the data in Fig. 9 reflect only the near surface smectic order. The sharp minimum at $Q_z/Q_0 \approx 1$ for 10CB is the only prominent feature in the data that is different for the three materials. In fact this may be somewhat of an accident in that for 10CB, at this particular value of Q_z/Q_0, the destructive interference between the amplitude of the x-ray reflected from the liquid crystal surface and that from the layers below is nearly complete.

Although all of this data has been modeled by guessing a form for the electron density $\langle\rho(z)\rangle$ and fitting it to the calculated form for $R(Q_z)/R_F(Q_z)$[60-63] an alternative method is to calculate the Patterson Function:

Eq. 15
$$P(s) = \int dQ_z \frac{R(Q_z)}{R_F(Q_z)} e^{-iQs} = \left(\frac{1}{\rho^\infty}\right)^2 \int dz dz' dQ_z \frac{\partial\langle\rho(z')\rangle}{\partial z'} \frac{\partial\langle\rho(z)\rangle}{\partial z} e^{i[z-z'-s]Q_z}$$
$$= \frac{2\pi}{[\rho^\infty]^2} \int dz \frac{\partial\langle\rho(z-s)\rangle}{\partial z} \frac{\partial\langle\rho(z)\rangle}{\partial z}.$$

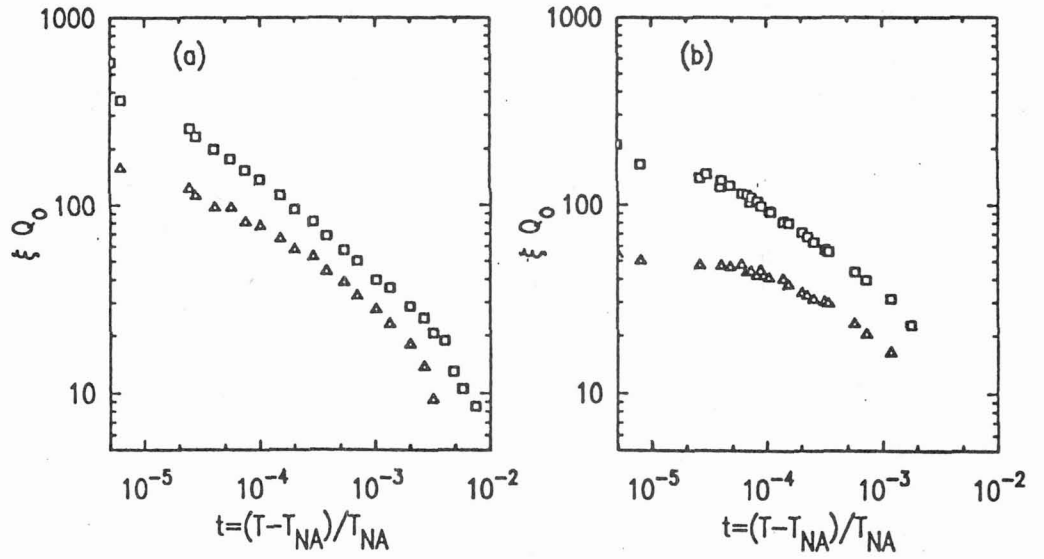

Fig. 8: Values of the surface penetration length $\xi(T)$ (□)and the bulk correlation length $\xi_{//}(T)$ (△) for (a)9.15CB and (b)9.30CB.[60-63]

The Patterson function calculated directly from the 12CB data in Fig. 9a is illustrated in Fig. 10a and one can immediately recognize 7 oscillations corresponding to that same number of surface induced layers. The real space density corresponding to this Patterson function has six oscillations of approximately 20% peak to peak amplitude followed by one more oscillation of about half that amplitude. Fig. 10b illustrates the real space density for the model whose Fourier transform gives rise to the solid line through the data in Fig. 9a. Although this model has only six prominent layers the calculated reflectivity is not very sensitive to the addition of another layer of smaller amplitude. The details of the sharp variation in electron density within each layer are also not unique. The important result is that by either method of analysis it is possible to obtain a measure of the number of surface layers to a precision of ±1 out of 6 or 7 layers and also a measure of relative amplitude of the electron density oscillations from layer to layer. The slight differences in the data shown in Fig. 9a for the different molecules

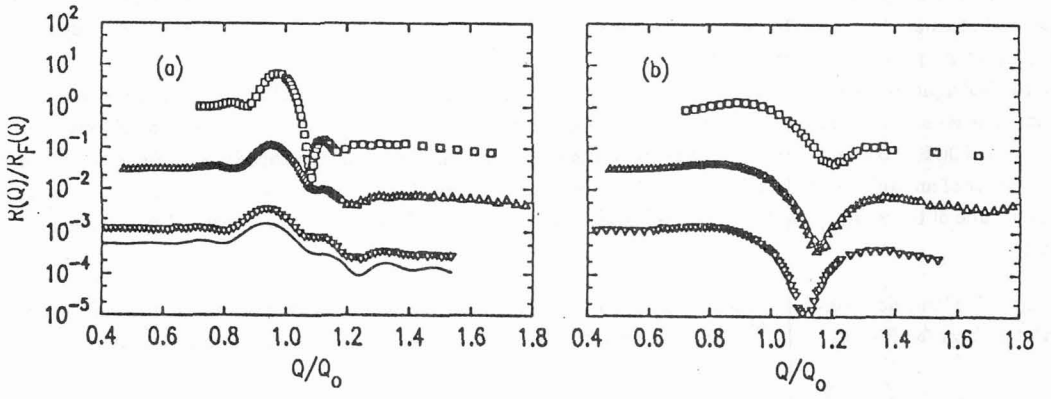

Fig. 9: $R(Q_z)/R_F(Q_z)$ as a function of Q_z/Q_o for (□)10CB,(△)11CB[60-63] and (▽)12CB[78] at (a)T-T_{IA} ~0.01°C and (b) at T-T_{IA} ~ 1.0°C. The solid line in (a), slightly displaced for visibility, from the 12CB data is obtained from the Fourier transform of the model real space density illustrated below in Fig. 10b.

might be explained by the fact that for 10CB it is possible to identify as many as eight well defined surface layers, while for both 11CB and 12CB it appears as though there are only six or seven.

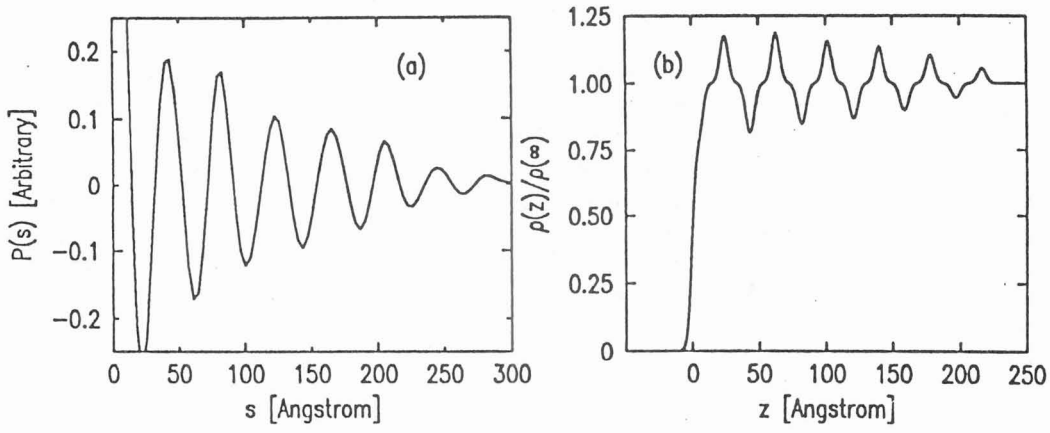

Fig. 10: (a) The Patterson function P(s) calculated by taking the Fourier transform of the 12CB data in Fig. 9a and (b) a real space model density whose Fourier transform is shown as the solid line in Fig. 9a.

The differences between the data shown in Fig. 9a at $T\text{-}T_{IA}$ for 0.01°C and Fig. 9b for 1.0°C is due to the fact that the number of surface layers change with temperature difference above the transition. This is demonstrated directly by fixing the spectrometer configuration at some Q_z near to the Q_0 for a particular material and measuring the intensity as a function of temperature. Fig. 11a displays such data for 10CB, 11CB and 12CB.

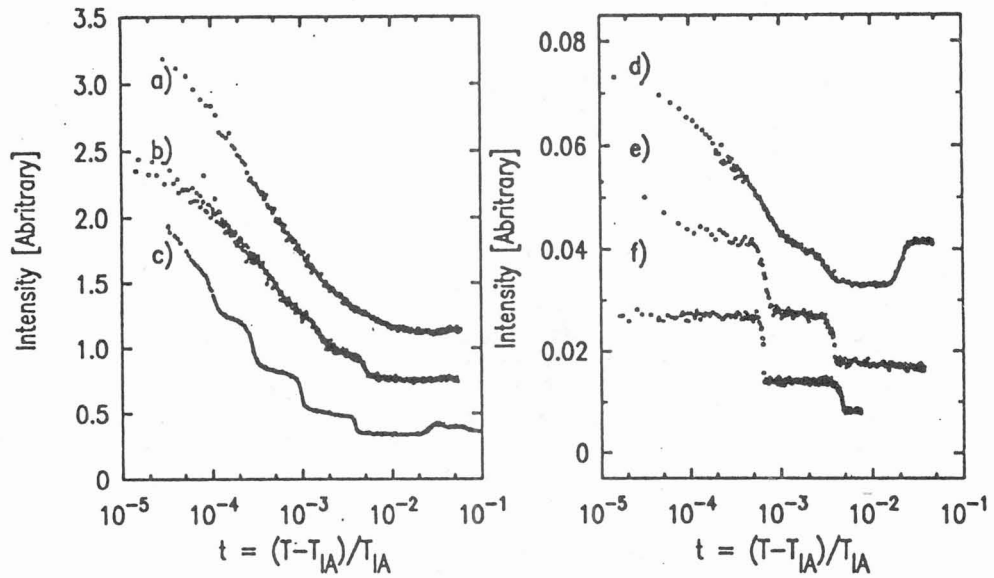

Fig. 11: (a)Reflected intensity as a function of reduced temperature $t = (T\text{-}T_{IA})/T_{IA}$ at $Q_z \approx Q_0$ for 10CB, 11CB and 12CB and (b) similar data for 12OCB, 14OCB and 16OCB.

On looking at this data it is tempting to suggest that the intensity is a measure of the number of surface layers and that they are diverging logarithmically as a function of reduced temperature $(T\text{-}T_{IA})/T_{IA}$. If this were true it

would correspond to complete wetting of the free isotropic surface by the smectic phase. In both the publication by Ocko et al[78] on 12CB, and in the unpublished work by Braslau et al[60-63] on 10CB and 11CB, the authors claimed the wetting was incomplete. However one regards those arguments, Fig. 11b displays similar data for three compounds from the nOCB and it is absolutely clear that in 16OBC the wetting is incomplete.[60-63]

Both the nCB and nOCB series exhibit the same tendency away from abrupt layering transitions as the alkane chains become shorter. As indicated by the phase diagram in Fig. 5 for nCB, the shorter chains are closer to the isotropic-nematic-smectic A triple point and we speculate that this implies that the response function of the isotropic phase for smectic order is also larger for the shorter chains. If this is true, then the increased response could smear out the interface between the surface induced smectic region and the bulk isotropic phase by either reducing the surface tension, thereby enhancing the roughness of the interface due to thermal roughening effects, or enhancing the smectic order in the isotropic phase. This would then be responsible for both the tendency away from abrupt layering transitions and also for the larger number of surface induced layers in 10CB than for 11CB and 12CB.

Surface Smectic A_1-A_2 Order

The above examples were chosen in order to emphasize the relation between liquid crystal surface phenomena and wetting in other systems. An interesting type of surface order which appears to be relatively unique to liquid crystals is the competition between smectic layering with two different length scales. We previously mentioned the fact that there are liquid crystalline systems in which the molecules seem to group together to form smectic A phases with layer thickness of the order of 1.6 × the molecular length. In other cases the fundamental layer thickness changes as a function of temperature and in one type of phase sequence there is a transition between a smectic A_1 phase, in which the layer spacing is equal to the molecular length, and a smectic A_2 phase in which the layer spacing is twice the molecular length.[79-82] Other cases, in which the layer spacing in the two phases are incommensurate, are also observed and in some materials there are temperatures where two incommensurate layer spacings coexist.

Fig. 12 displays $R(Q_z)/R_F(Q_z)$ at two temperatures for a compound known as DB_7NO_2 for which there is

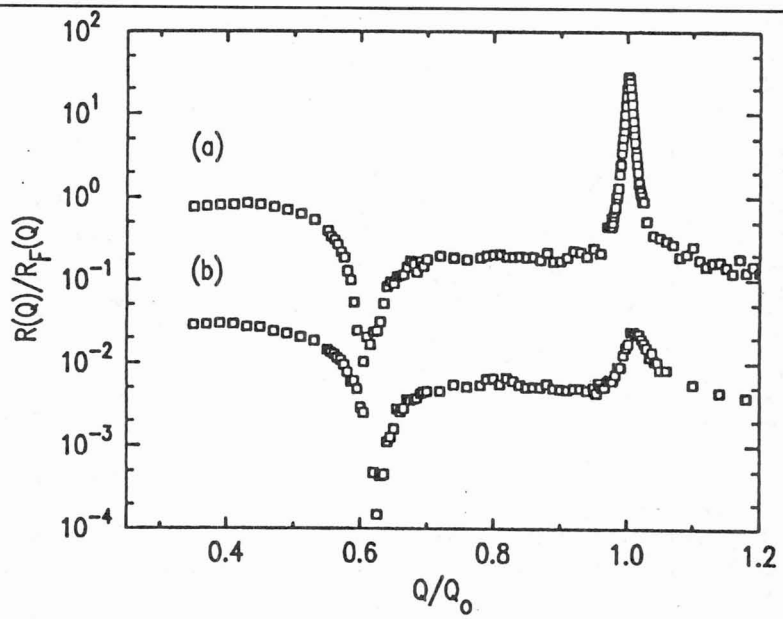

Fig. 12: $R(Q_z)/R_F(Q_z)$ as a function of Q_z/Q_0 for a molecule DB_7NO_2 with two incommensurate coexisting density waves at (a)$\Delta T=T-T_{NA}$ = 0.6°C and (b) 4.6°C.

coexistence in the bulk nematic phase between smectic fluctuations with wave vectors $Q_o \approx 2\pi$/Molecular length and $Q_d \approx 0.6Q_o$.(83) In this material there is a 2nd order nematic to smectic phase transition in which the correlation lengths $\xi_{//}$ and $\xi_{\perp}$ associated with the order at wavevector Q_o diverge while the correlation lengths associated with Q_d, although temperature dependent, remain finite. The data in Fig. 12 show surface structure at both Q_o and $Q_d \approx 0.6Q_o$ but with interference effects that are nearly 180° out of phase with each other. Analysis of this, and other data, indicates that the surface and bulk correlation lengths associated with the peak at Q_o appear to be equal to each other, both diverging as the $T \rightarrow T_{NA}$. In contrast the surface penetration length associated with Q_d is smaller than the bulk correlation length by a temperature dependent factor between 3 and 4. This is another example where the surface and bulk lengths are different. Gramsbegen et al have studied a similar compound in which $Q_d = Q_o/2$ and have obtained similar results.(84,85)

Lyotropic Smectic A Order

Fig. 13a,b displays $R(Q_z)/R_F(Q_z)$ for mixtures of CsPFO and H_2O containing approximately 60% weight H_2O at two temperatures. As was mentioned above, this system is known to form a bulk phase of oblate micelles.(76) There is approximately a 6°C range of temperatures over which these micelles orient to form a birefringent lyotropic nematic phase. At higher temperatures the solution is isotropic and at lower temperatures it is smectic A. The peak in the specular reflectivity clearly indicates a temperature dependent surface layering and Fig. 13c displays one model for the electron density that is consistent with the observed reflectivity. Analysis of this data is currently in progress and this may not be the optimum model, however the preliminary results have two very interesting features.

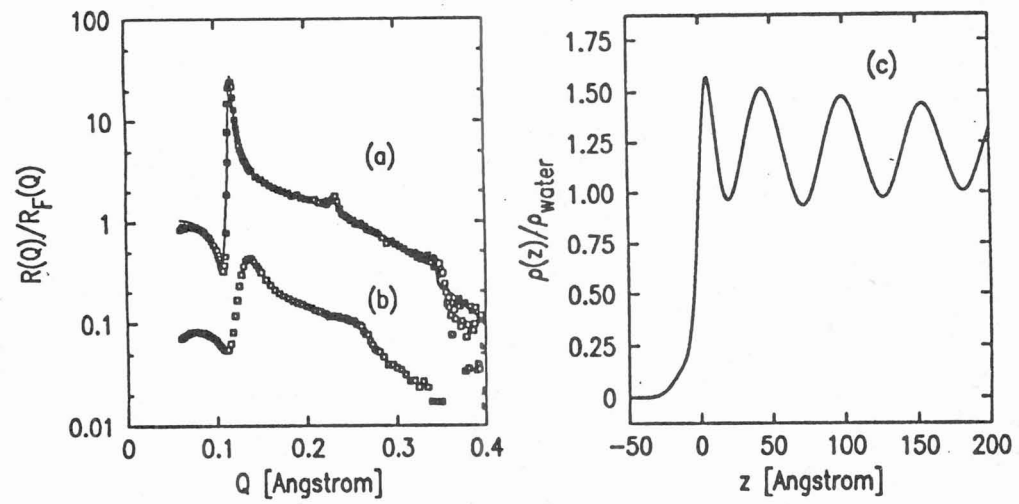

Fig. 13: $R(Q_z)/R_F(Q_z)$ from the surface of a mixture CsPFO and H_2O (approximately 60 wt % H_2O) in the temperature range where the bulk is (a) in the nematic phase, approximately 2°C above the transition temperature T_{NA} to the smectic A phase, and (b) in the isotropic phase approximately 7°C above T_{NA}. The data are represented by (o) and the solid line is the ratio $R(Q_z)/R_F(Q_z)$ predicted by the model electron density profiles shown in (c).(86)

Firstly, the peak in the electron density at the surface near $z \approx 0$ is roughly half as wide as that of the subsequent maxima. Since the full width at half maximum of the subsequent maxima are approximately twice the molecular length of the CsPFO molecule (i.e. ≈ 12.5Å) this suggests that the region near to the surface consists of a surface monolayer of CsPFO followed by either layers of oblate micelles with their short dimension along the layer normal, or by fully formed layers of bilayers. The second important feature of this model is that the electron

density oscillates between a minimum value that is very close to that of pure H_2O and a maximum that is approximately 1.5 that of H_2O. This argues that the whether the layers nearest to the surface are actually relatively well formed bilayers or layers of small micelles they are separated by water layers that are relatively free of CsPFO molecules. The maximum value of 1.5 is significantly smaller than the density of approximately 2 times that of H_2O that is obtained using the molecular volume for CsPFO of 360Å^3 that was quoted by Boden at al.[76] One explanation for this lower density is that the near surface layers were made up of layers of micelles separated by suitable intralayer H_2O regions. On the other hand the density of the surface monolayer is essentially the same as that of the layers below the surface and it is not obvious how to form a surface monolayer from micelles. If we assume a homogeneous surface monolayer with an electron density of the order of 1.5 times that of H_2O (or 75% of the value calculated by dividing the total number of electrons by the molecular volume) then it is possible that the near surface layers are bilayers with this same density. Fig. 6b illustrates this possibility. In this model the position of the cross over from lamallae to micelles might be temperature dependent.

Thermotropic In-Plane Order

Finally, and primarily for completeness, we mention surface effects relating to an in-plane order parameter parallel to the free surface. On cooling below the smectic A phase many liquid crystalline molecules will form bulk liquid crystalline phases such as the hexatic B, the smectic I and F, with hexatic in-plane order.(1,2) The hexatic B is a normal uniaxial hexatic but the latter two phases are optically biaxial with the molecules tilted away from the layer normal. Examples of other phases are the crystalline B, G and J which are true 3-dimensional crystals, although with very weak interlayer coupling. In 1978 Young, Pindak, Clark and Meyer,(28,29) resurrecting an old idea of Friedel,(87) demonstrated that it is possible to form relatively stable freely suspended smectic films as thin as two molecular layers and suggested them as natural systems in which to study structural phase transitions in two dimensions. There is not sufficient space in this article to completely review all of the x-ray scattering experiments on freely suspended films that followed the pioneering experiment by Moncton and Pindak(24), and we will simply show in Fig. 14 a set of scans along a reciprocal space direction parallel to the surface of a 5 molecular layer thick film of the liquid crystal 7O.7 for three different temperatures. The data in

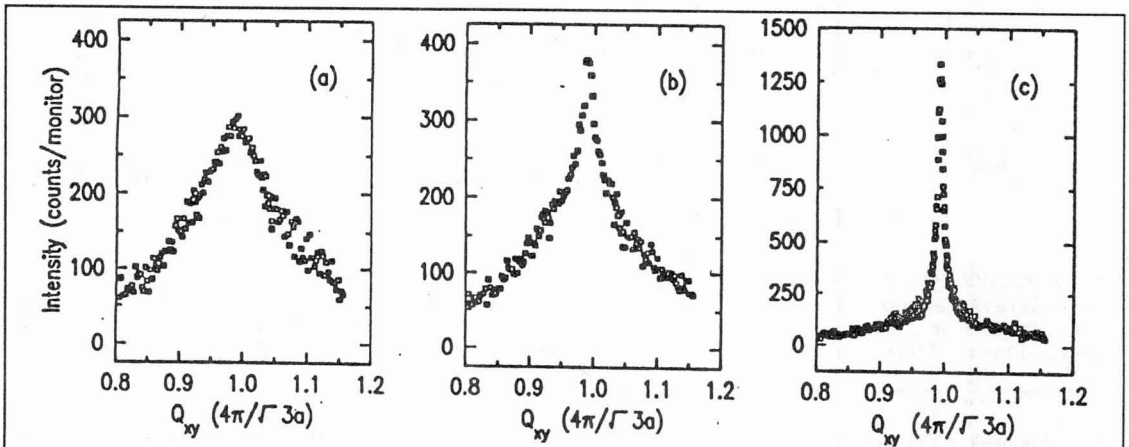

Fig. 14. X-ray scattering spectra from a freely suspended 5-layer thick film of 7O.7 for temperatures where the entire film is (a)smectic C, T=78.14°C; (b) where the two surface layers have formed a tilted hexatic smectic I phase and the interior are smectic C, T=77.67°C; and (c) where all five layers are smectic I, T=69.07°C.(88)

Fig. 14a displays a broad diffuse peak corresponding to the liquid like order of of the smectic C phase at T=78.14°C. The data in Fig. 14b is the superposition of a sharper central peak, from the two surface layers that have formed a tilted hexatic smectic I phase, and a broader diffuse peak, from the three interior layers that are still smectic C, at T=77.67°C. The data in Fig. 14c correspond to a lower temperature in which all five layers in the film are smectic I at T=60.09°C.(88)

In this system the smectic I does not wet the surface and there is a first order transition at which the interior layers become smectic I. More recent experiments by L. B. Sorensen et al indicate that layer by layer freezing can be observed for free films of the molecule 9O.4 out to nearly 30 molecular layers.(89) It is likely that this is a case of complete wetting.

Conclusion

In summary we have demonstrated the manner in which specular reflectivity of x-rays can be used to investigate the structure along the normal to the surface for both liquids and liquid crystals. The most striking feature is the tendency of the surfaces of all of these systems to induce smectic like layers that decay with distance from the surface. For temperatures above a 2nd order nematic to smectic A phase transition the surface induced layering generally extends exponentially into the bulk with a characteristic length that is equal to the bulk correlation length $\xi_{//}$. Since $\xi_{//}$ diverges a $T \rightarrow T_{NA}$ this can be classified as critical adsorption. When the nematic to smectic A transition is 1st order the surface induced ordering penetrates further than $\xi_{//}$ and the data implies that there may be a true wetting transition along the line of 1st order nematic to smectic A transitions on approaching the tricritical point where the transition becomes 2nd order. The surface of the isotropic phase, near to a 1st order transition to the smectic A phase exhibits layering transitions and at least one clear example of incomplete wetting has been demonstrated. Along the line of 1st order isotropic to smectic A transitions, near to the triple point where the isotropic, nematic, and smectic A phases coexist, the data suggest the possibility of a roughening transition for the interface between the surface induced smectic and the isotropic phase. Further experiments will be necessary to fully understand all of these features.

We have also presented data from the surface of one lyotropic liquid crystal (CsPFO) demonstrating homogeneous surface induced bilayers at temperatures in which the bulk phase consists of finite size micelles. This is qualitatively different from surface structure seen in a different lyotropic system and serves to emphasize that our understanding of the surface properties of these solutions is at a very primitive stage.(90)

Finally, we have presented one liquid crystal example of surface induced order within the plane of the surface. The example was chosen to illustrate the fact that since liquid crystals form stable, free standing, thin films structural studies of surface phenomena can be carried out in a transmission geometry rather than in grazing incidence.

Acknowledgements

This work was supported by the National Science Foundation through grants to the Harvard Materials Research Laboratory, NSF-DMR-85-13523 and NSF-DMR-85-13523-86-14003. Research carried out at the NSLS, Brookhaven National Laboratory, is supported by the Department of Energy, Material Sciences and Division of Chemical Sciences under contract DE-AC02-76CH00016.

References

/1/ P. S. Pershan, *World Scientific Lecture Notes in Physics-Vol. 23 Structure of Liquid Crystal Phases* (World Scientific, Singapore, 1988)

/2/ G. W. Gray and J. W. Goodby, *Smectic Liquid Crystals, Textures and Structures* (Leonard Hill, Glasgow, 1984)

/3/ K. Miyano, Phys. Rev. Lett. 43, 51(1979); J. Chem. Phys. 71, 4108(1979).

/4/ D. Beaglehole, Mol. Cryst. Liq. Cryst. 89, 319(1982).

/5/ T.J. Suckin and A. Poniewierski, in *Fluid Interfacial Phenomema*, Ed. C. A. Croxton (Wiley, NY, 1986), p215.

/6/ F. J. Kahn, Appl. Phys. Lett. 22, 386(1973).

/7/ R.Evans, Adv. in Phys. 28, 143(1979).

/8/ R. Pandit, M. Schick , and M. Wortis , Phys. Rev. B 26 , 5112 (1982).

/9/ A. Croxton,*Statistical Mechanics of the Liquid Surface* (John Wiley and Sons,N.Y.,1980)

/10/ P.G. de Gennes, Rev. of Mod. Phys. 57 , 827 (1985).

/11/ A. H. Compton, Bull. Nat. Res. Coun. (US) 20, 48 (1922).

/12/ L. G. Parratt, Phys. Rev. 95, 359 (1954).

/13/ L. Bosio and M. Oumezine, J. Chem Phys. 80, 959 (1984).

/14/ S.A. Rice, Nature 316, 108(1985)

/15/ J. Als-Nielsen, F. Christensen , and P.S. Pershan ,Phys. Rev. Lett. 48, 1107 (1982).

/16/ P. S. Pershan , and J. Als-Nielsen , Phys. Rev. Lett. 52 , 759 (1984).

/17/ J. Als-Nielsen, Physica 140A, 376 (1986).

/18/ P. S. Pershan, A. Braslau, A. H. Weiss, and J. Als-Nielsen, Phys. Rev. A35,, 4800(1987)

/19/ W. Burton, N. Cabrera, and F. C. Frank, Phil. Trans. Roy. Soc. A243, 299 and 315(1951).

/20/ *Ordering in Two Dimensions,* (North Holland, N.Y., 1980), Ed.S. Sinha.

/21/ J. G. Dash, Physics Today 38, 26(1985).

/22/ M. Schick, in *Liquids at Interfaces, Les Houces Summer School Lectures*, Session XLVIII.

/23/ S. Dietrich, in *Phase Transitions and Critical Phenomena*, (Academic, London, 1988), Ed. C. Domb and J. Lebowitz.

/24/ D.E. Moncton, R. Pindak, S.C. Davey, and G.S. Brown , Phys. Rev. Lett. 49 , 1865 (1982).

/25/ S.C. Davey, J. Budai, J. W. Goodby, R. Pindak, and D.E. Moncton, Phys. Rev. Lett. 53, 2129 (1984).

/26/ E.B. Sirota, P.S. Pershan, L.B. Sorensen, and J. Collett, Phys. Rev. Lett.55, 2039 (1985).

/27/ J.D.Brock, ,A. Aharony, R.J. Birgeneau, K.W. Evans-Lutterodt, J.D. Litster, P.M. Horn, G.B. Stephenson, and A.R. Tajbakhsh, Phys. Rev. Lett. 57, 98 (1986).

/28/ C. Y. Young, R. Pindak, N. A. Clark, and R. B. Meyer, Phys. Rev. Let. 40, 773(1978)

/29/ C. Rosenblatt, R. Pindak, N.A. Clark, and R.B. Meyer, Phys. Rev. Lett. 42 , 1220 (1979).

/30/ E.B. Sirota, P.S. Pershan, L.B. Sorensen, and J. Collett, Phys. Rev. A36, 2890 (1987).

/31/ B. C. Lu and S. A. Rice, J. Chem Phys. 68, 5558(1978)

/32/ L. Bosio, and M. Oumezine, J. Chem. Phys., 80, 959(1984)

/33/ J. Als-Nielsen and P.S. Pershan , Nuclear Inst. & Methods, 208, 545(1983)

/34/ A.H. Weiss, M. Deutsch, A. Braslau, B.M. Ocko, and P.S. Pershan, Rev. Sci Inst., 57, 2554 (1986).

/35/ P. Beckmann and A. Spizzichino, in *The Scattering of Electromagnetic Waves From Rough Surfaces*, (Pergamon, New York, 1963).

/36/ A. Braslau, M. Deutsch, P.S. Pershan, A.H. Weiss, J. AlsNielsen, and J. Bohr, Phys. Rev. Lett., 54, 114. (1985).

/37/ A. Braslau, P. S. Pershan, G. Swislow, B. M. Ocko, and J. Als-Nielsen, Phys. Rev. A, 38, 2457(1988)

/38/ Y. Yoneda, Phys. Rev. 131, 2010 (1963).

/39/ O.J. Guentert, J. Appl. Phys. 36, 1361 (1965).

/40/ Y. Wangand W. L. Wolfe, J. Opt. Soc. Am.73, 1596 (1973); Proc. of the SPIE 257, 223 (1980).

/41/ B. Aschenbach, H. Brauninger, A. Ondrusch, and P. Predehl, Proc. of the SPIE 316, 187 (1981).

/42/ D. Schwartz, M. Schlossman, E. Kawamotro, G. Kellogg, and P.S. Pershan (1989). Unpublished. This recent result is from measurements on the surface of water that was maintained free of impurities. See ref. 36 and 37 for earlier measurements.

/43/ J. Daillant, J. J. Benattar, L. Bosio, and L. Leger, "Final stages of spreading of polymer droplets on smooth solid surfaces," Euro. Phys. Lett. 8, 453(1989).

/44/ Theory predicts that the height-height correlations due to thermal capillary waves increase logarithmically with distance. As a consequence the mean square value for the measured roughness σ^2 also depends logarithmically on the spectrometer resolution, or the size of the detector slit shown in Fig. 2. See ref. 37 for further details.

/45/ *Liquid Crystal Devices* , (Optosonic Press, New York, 1973) Ed. T. Kallard.

/46/ *The Physics and Chemistry of Liquid Crystal Devices*, (Plenum Press, 1980) Ed. G. J. Sprokel.

/47/ G. W. Smith, Z. G. Gardlung, and R. J. Curtis, Mol. Cryst. Liq. Cryst. 19, 327(1973).

/48/ J. Thoen, H. Marynissen, and W. Van Dael, Phys. Rev. Lett., 52, 204 (1984)

/49/ W. Maier and A. Saupe, Z. Naturf. A13, 564(1958); A14, 882(1959);

/50/ A. Stroobants, H. N. W. Lekkerkerker, andD. Frenkel, Phys. Rev. Lett., 57, 1452(1986)

/51/ Xin Wen, and R. B. Meyer, Phys. Rev. Lett. 59, 1325(1987)

/52/ J. Als-Nielsen, R.J. Birgeneau, M. Kaplan, J.D. Litster , and C.R. Safinya, Phys. Rev. Lett. 39 , 352 (1977).

/53/ C.W. Garland, M. Meichle, B.M. Ocko, A.R. Kortan, C.R. Safinya, L.J. Yu, J.D. Litster , and R.J. Birgeneau, Phys. Rev. 27 , 3234 (1983).

/54/ B. M. Ocko, R.J. Birgeneau, and J.D. Litster, Z. Physik B62, 487 (1986).

/55/ G.W. Gray and J. E. Lydon, Nature (London) 252, 221(1974).

/56/ P.E. Cladis, R. K. Bogardus and D. Aadsen, Phys. Rev. A18, 2292(1978).

/57/ P. G. de Gennes, *The Physics of Liquid Crystals* (Clarendon, Oxford, 1974).

/58/ T. C. Lubensky , J. Chem. Physique, 80, 31(1983).

/59/ Transition temperatures for the nOCB series are taken from commercial publications of the British Drug House, Ltd. Broom Road,Poole, England.

/60/ A. Braslau, B. M. Ocko, P. S. Pershan, Bull. Am. Phys. Soc., 32,474(1987)

/61/ B. M. Ocko, A. Braslau, P.S. Pershan, D. K. Schwartz and G. Swislow, Bull.Am. Phys. Soc., 32,474(1987

/62/ Alan Braslau, Ph.D. Thesis, Harvard University, 1988(unpublished)

/63/ P. Sheng, Phys. Rev.A26, 1610 (1982); Phys. Rev. Lett. 37 , 1059(1976).

/64/ J. V.Selinger, Jonathan V., Phys. Rev.A37, 1736 (1988).

/65/ D. Ronis and C. Rosenblatt, Phys. Rev. A21, 1687(1980).

/66/ C. Rosenblatt, Phys. Rev. A23, 305(1981).

/67/ Z. Pawlowska, G. F. Kventsel and T. J. Sluckin, Phys. Rev. A36, 992(1987).

/68/ Although recent theories (ref 50 and 51) do predict smectic A order for "hard rod models" the relative importance of steric effects, in comparison with dynamical effects due to the alkyl chains and anisotropic attractive interactions between neighboring molecules is not yet clear.

/69/ P. Guyot-Sionnest, P., H. Hsiung, and Y. R. Shen, Phys. Rev. Lett.,57, 2963 (1986).

/70/ H. Hsiung, Th. Rasing, and Y. R. Shen, Phys. Rev. Lett.,57, 3065 (1986).

/71/ P.S. Pershan, J. de Physique Colloq. 40, C3-423 (1979)

/72/ P.S. Pershan, Physics Today 35, 2 (1982).

/73/ *Physics of Complex and Supermolecular Fluids* , (Wiley, NY, 1987), Ed. S. A. Safron and N. A. Clark.

/74/ M. C. Holmes and J. Charvolin,J. Phys. Chem. 88, 810(1984).

/75/ J. Charvolin, J. Chim. Phys. 80, 15(1983)

/76/ N. Boden, S. A. Corne, M. C. Holmes, P. H. Jackson, D. Parker, and K.W. Jolley, J. Phys.(Paris) 47, 2135 (1986).

/77/ M.R. Fisch, S. Kumar, and J.D. Litster, vol. 57, 2830 (1986).

/78/ B. M. Ocko, A. Braslau, P. S. Pershan, J. Als-Nielsen, and M. Deutsch, Phys. Rev. Lett. 57, 94(1986)

/79/ J. Prost, Adv. Phys. 33, 1(1984)

/80/ J. Wang and T. Lubensky , Phys. Rev. A29, 2210 (1984)

/81/ A. M. Levelut, R. J. Tarento, F. Hardouin, M. F. Achard and G. Sigaud, Phys. Rev. A24, 2180(1981).

/82/ B. R. Ratna, R. Shashidhar and V. N. Raja, Phys. Rev. Let. 55, 1476 (1985).

/83/ B. M. Ocko, P.S. Pershan, C.R. Safinya and L.Y. Chiang, Phys. Rev. A35, 1868(1987).

/84/ E. F. Gransbergen, W.H. de Jeu, and J. Als-Nielsen, J. Phys. (Paris), 47, 711, (1986).

/85/ E.F.Gransbergen, and W.H. de Jeu, J. Phys. (Paris), 49, 33 (1988)

/86/ G. Swislow, B. M. Ocko, D. K. Schwartz, A. Braslau and P. S. Pershan(unpublished). See Bull. Am. Phys. Soc. 32, 902(1987).

/87/ G. Friedel, Annls. Phys. 18, 273 (1922).

/88/ S. Amador, P.S. Pershan, H. Stragier, B.D. Swanson, D.J. Tweet, L.B. Sorensen, E.B. Sirota, G.E. Ice, and A. Habenschuss, Phys. Rev. A39, 2703(1989).

/89/ B. D. Swanson, H. Stragier, D. J. Tweet, and L. B. Sorensent, Phys. Rev. Let. 62, 909(1989).

/90/ D. Schwartz, A. Braslau, B. Ocko, P.S. Pershan, J. Als-Nielsen, and J.S. Huang, Phys. Rev. A38, 5817(1988)